AIAA JOURNAL
Vol. 51, No. 7, July 2013

A General Theory of Flow-Instability Inception in Turbomachinery

Xiaofeng Sun* and Xiaohua Liu†
Beihang University, 100191 Beijing, People's Republic of China
Ruiwei Hou‡
Shenyang Aeroengine Research Institute, 110015 Liaoning, People's Republic of China
and
Dakun Sun§
Beihang University, 100191 Beijing, People's Republic of China

DOI: 10.2514/1.J052186

A general eigenvalue theory on flow stability in turbomachinery is proposed with the emphasis on flow-instability onset. Based on this theory, a stall-inception model including the effects of complex solid geometry is developed for a multistage fan/compressors system. The capacity of the present model to predict the stall-inception point is assessed against experimental data of both a low-speed and transonic single rotor. Comparisons with a simplified two-dimensional model are performed to identify the nonnegligible effects of spanwise distribution of flowfield in a general configuration on the unstable mode of the concerned fan/compressors. It is verified that this model is capable of predicting mass flow at the stall-onset point of both subsonic and transonic flow with a reasonable accuracy, and it is sustainable in terms of computation cost for industrial application.

Nomenclature

$\boldsymbol{A}, \boldsymbol{B}, \boldsymbol{C}, \boldsymbol{D}, \boldsymbol{G}, \boldsymbol{H}, \boldsymbol{Q}, \boldsymbol{X}$	=	coefficient matrix
c_j	=	constant coefficient
c_v	=	specific heat at constant volume
D_r	=	radial partial derivative
D_{rr}	=	radial second-order partial derivative
D_{rz}	=	radial and axial mixed second-order partial derivative
D_s	=	partial derivative on streamline coordinate
D_z	=	axial partial derivative
D_{zz}	=	axial second-order partial derivative
E	=	total energy
F	=	body force scalar
$\mathbf{F}$	=	body force vector
F_t	=	body force component parallel to the mean camber surface of blades in blade-to-blade surface
F_v	=	body force component normal to the mean camber surface of blades in blade-to-blade surface
f, g	=	smooth function on computational plane
f_z	=	unsteady force in axial direction
f_θ	=	unsteady force in circumferential direction
i	=	imaginary unit
K	=	dimensionality of matrix
k	=	heat transfer coefficient
k_c	=	undetermined body force coefficient
M, N	=	integer
m	=	circumferential mode number
n	=	normal to streamline coordinate in meridian plane
p	=	static pressure
p_t	=	stagnation pressure
$\bar{p}_t$	=	rotary stagnation pressure
$\hat{q}$	=	heat volumic source by unit of mass, W/kg
R	=	gas constant
r, θ, z	=	cylindrical coordinates
r_t	=	radius at the tip of the leading edge
s	=	streamline coordinate
T	=	temperature
T_N	=	N-order Chebyshev polynomial
t	=	time
$\boldsymbol{U}$	=	column-orthogonal matrix
U_0	=	axial velocity of incoming flow at inlet
$\boldsymbol{V}$	=	orthogonal matrix
V	=	velocity scalar
$\mathbf{V}$	=	velocity vector
v'	=	fluctuation velocity scalar
$\boldsymbol{W}$	=	diagonal matrix
β	=	circumferential metal angle of the mean camber surface in surface (θ, z)
γ	=	specific heat ratio
λ	=	loss coefficient
ε	=	body force coefficient
ζ, η	=	rectangular coordinates in computational plane
μ	=	dynamic viscosity coefficient
ρ	=	density
$\boldsymbol{\tau}$	=	viscous stress tensor
τ	=	time-delay constant
$\boldsymbol{\Phi}$	=	column vector of perturbation amplitudes
Ω	=	rotational speed of rotor, rpm
ω	=	eigenfrequency of the fan/compressors system
ω_r	=	real part of eigenfrequency
ω_i	=	imaginary part of eigenfrequency

Subscripts

a, b	=	points along one streamline
i, j	=	integer
r, θ, z	=	radial, circumferential, and axial component
t	=	stagnation property

Superscripts

T	=	transpose of matrix

Presented as Paper 2012-4156 at the 48th AIAA/ASME/SAE/ASEE Joint Propulsion Conference & Exhibit, Atlanta, Georgia, 30 July–1 August 2012; received 1 July 2012; revision received 14 December 2012; accepted for publication 17 December 2012; published online 9 April 2013.

*Professor, School of Jet Propulsion; Sunxf@buaa.edu.cn.
†Ph.D. Candidate, School of Jet Propulsion; Liuxh@sjp.buaa.edu.cn.
‡Ph.D., Compressor Department; Hrw407@gmail.com.
§Ph.D., School of Jet Propulsion; Renshengming@sjp.buaa.edu.cn.

I. Introduction

FLOW instability is one of the most severe challenges for turbomachinery. As one major type, rotating stall is a natural limit to the performance of the fan/compressors, which could cause catastrophic damage to the whole fan/compressors system. Much progress has been achieved on studying this issue during the past few decades. In 1976, Greitzer [1] presented a stability model of compressor system, which can not only be used to predict the onset condition of stall and surge but also to study the nonlinear development of stall cells. Garnier et al. [2] demonstrated that modal disturbance rotates around the annulus during the stalling process. Experiments performed by McDougall et al. [3] and Day [4] first confirmed the existence of two types of stall precursors: modal wave and spike. In the following years, considerable experimental work (Camp and Day [5], Day et al. [6], Wilson and Freeman [7], Tryfonidis et al. [8], etc.) was conducted to investigate the evolution process of rotating stall. Day et al. [6] experimentally studied on four high-speed compressor rigs and observed two new phenomena for the first time: fixed-location stall and high-frequency stall. It is of great interest that multiple types of stall precursors exist at the same time or trigger reciprocally during the stalling process [5]. Furthermore, inlet distortion, Reynolds number, and stage mismatching also affect the route to stall. In a word, it is revealed that a variety of stall routes are involved in different compressors, and the actual stalling patterns of one specific fan/compressors in different operating conditions are also various and complicated.

Although a unified theory that could explain all varieties of detailed stalling process remains some way off, it is evident that all types of stall precursor grow from a small oscillation to developed stall cell. Despite the significance of research on the detailed development process of stall precursor, it is the position of the instability onset point that concerns engineers primarily. There are generally two different types of work to study the stall inception of the fan/compressors. The first, known as analytical models, mostly describe flow stability as an eigenvalue problem by simplifying flowfield and placing emphasis on stall-inception period when the flow perturbation is small and linear assumption is suitable. The work of Nenni and Ludwig [9] extended the channel-flow theory proposed by Sears [10] and resulted in an analytical expression for the inception condition of rotating stall. Takata and Nagashima [11] studied the rotating stall in three-dimensional (3-D) blade rows with emphasis on the effects of nonuniform flow or shear flow on the stall inception. Gordon [12] presented a 3-D incompressible stability model to study the stall onset for general fan/compressors structure. Sun [13] developed a 3-D compressible stability model including the effects of casing treatment, and this work was recently extended to transonic compressor stability [14]. It is verified that most analytical models can predict the instability inception point with satisfactory accuracy as long as sufficient loss and performance characteristics of the concerned fan/compressors are given. The second type of work, numerical calculation, which is developing rapidly in recent years with the increasing availability of computing power, is to directly solve unsteady Euler or Navier–Stokes (N–S) equations as an initial boundary-value problem to obtain the information related to stalling evolution. Owing to multiple time and length scales involved in rotating stall, direct time-accurate numerical calculation by unsteady Reynolds-averaged Navier–Stokes (RANS) equations on full annulus grids is unacceptable for industrial applications in terms of unsustainable computational cost. He [15] conducted a computational study on stall inception using a quasi-three-dimensional time-marching N–S equations method and successfully simulated single-cell and multiple-cell pattern stall. Escuret and Garnier [16], Longley [17], and Chima [18] employed the body-force approach to represent the effects of blades on the flowfield and computed the stalling process. Hoying et al. [19] performed numerical calculations on an eight-blade passage rotor to compute the flowfield before stall, and the simulation gave an insight into the physical origin of stall precursor. Gong et al. [20] made the first effort to simulate 3-D nonlinear development of stall precursor in multistage compressors. Gourdain et al. [21] solved quasi-three-dimensional N–S equations on a stream surface and identified the spatial mode of flow disturbance before stall inception by using Fourier analysis.

Numerical approach has an advantage over analytical models in that it can consider the effects of more aerodynamic and geometry parameters on the physical process involved in rotating stall. However, it is vital for an initial boundary-value problem to determine how to introduce the initial perturbations outside or inside the computational domain to stimulate the stall precursor. Because of the unsteadiness, turbulence, and complicated configuration, there are extremely plentiful of disturbance in terms of frequency, amplitude, and length scale in the actual flowfield of the fan/compressors during the whole stalling process. This diversity of disturbance makes an inevitable trouble to this approach, and there are not common rules yet to be followed to overcome this challenge. Nevertheless, it is noted that the stability of a dynamic system depends on its response to any initial small perturbation inside and outside the system rather than some specific perturbation. It is evident that flow perturbation always grows via a development process from small to large in most flow-stability problems. If emphasis is placed on the inception period of flow instability, linearization is a reliable technique, and theoretically all flow-instability inception problems can be described as an eigenvalue equation based on N–S equations. Take the research on the boundary layer transition for instance. There exists a variety of routes to deal with this problem, and the Orr–Sommerfeld equation is one resultful theory. An integrated procedure for solving this issue is provided as follows. First, the flow velocity profile with some certain Reynolds number is computed by steady computational fluid dynamics (CFD) calculation. Under the assumptions of small perturbation and uniform shear flow, a four-order ordinary differential equation is established. After solving the Orr–Sommerfeld equation with appropriate boundary conditions, the most unstable disturbance can be judged by the imaginary part of resultant complex eigenfrequency. Meanwhile, the most unstable mode may provide an appropriate initial perturbation to the initial boundary-value problem for further inquiry on the nonlinear stage of boundary flow transition. As a matter of fact, most of earlier analytical models in studies of rotating stall were to establish various eigenvalue equations with emphasis on stall inception. To facilitate the analytical solution of the flowfield, a variety of simplification and assumptions are made in these models. The prediction result of these models depends on the accuracy of the fan/compressors characteristics, which is not generally known with great precision, especially during the design phase of new fan/compressors without sufficient empirical correlations. Numerous requirements for loss and deviation angles restrict the practical application of these simplified models.

Many researchers (Jacobs and Sherman [22], Abbott and von Doenhoff [23], Rusak [24], Rusak and Morris [25], etc.) have made a great deal of progress on stall onset of an airfoil. It is without doubt that the study on the stall inception of compressors will benefit from the physical understanding of the airfoil stall problem. However, rotating stall of compressors is related to not only the sudden flow separation and loss of lift on the blades but also the interactive effects of adjacent blade rows and the propagation of flow disturbance around the annulus. Under this circumstance, many flow details on cascade have to be neglected in the rotating stall-inception model. An alternative and simplified approach is therefore required. In conclusion, although a great deal of progress has been made on the mechanism of flow stability, little research has been conducted on instability inception of compressible flow including the effects of complex configuration of the fan/compressors. Additionally, there is currently not yet an effective methodology for providing an unambiguous judgment on the stall-onset point during the fan/compressors design phase. It is the lack of such a capability that motivated the authors to develop a new flow-instability inception model in this paper. The main purpose of this investigation is summarized as follows.

1) Propose a methodology for stall-onset prediction during the fan/compressors design stage, and assess the feasibility for both subsonic and transonic flow.

2) Identify the necessity of developing 3-D compressible flow-stability model for getting an accurate stall margin prediction.

3) Provide the most unstable mode of the fan/compressors system for further research on the nonlinear development of stall precursor.

In this paper, a general eigenvalue theory on 3-D compressible flow stability is proposed. In consideration of rotating stall inception, the mean flowfield of the fan/compressors is computed by RANS calculation. Then, a body-force model is suggested, which represents the effects of blades on the flowfield. Further, by applying appropriate boundary conditions and spectral collocation method, a group of homogeneous equations will yield, from which a stability equation can be finally derived. After solving this eigenvalue equation using singular value decomposition (SVD) over a fine grid of eigenfrequency, the onset point of flow instability can be judged by the imaginary part of resultant eigenvalue. Finally, model assessments are performed on two compressors, and the results verify that this model is capable of predicting the stall-onset point of both low-speed and transonic fan/compressors flow.

II. A General Eigenvalue Theory on Flow-Instability Inception

A general eigenvalue theory on 3-D compressible flow stability is proposed in this section, which is described as an eigenvalue equation based on N–S equations as follows:

$$\frac{\partial \rho}{\partial t} + \nabla \cdot (\rho \mathbf{V}) = 0 \tag{1}$$

$$\frac{\partial \rho \mathbf{V}}{\partial t} + \nabla \cdot (\rho \mathbf{V}\mathbf{V}) = \rho \mathbf{F} - \nabla p + \nabla \cdot \tau \tag{2}$$

$$\frac{\partial \rho E}{\partial t} + \nabla \cdot (\rho \mathbf{V} E) = \rho \mathbf{F} \cdot \mathbf{V} - \nabla \cdot (p\mathbf{V}) + \nabla \cdot (\tau \cdot \mathbf{V}) + \rho \hat{q} + \nabla \cdot (k \nabla T) \tag{3}$$

$$\nabla \cdot \boldsymbol{\tau} = \mu \Delta \mathbf{V} + \frac{1}{3}\mu \nabla (\nabla \cdot \mathbf{V}) \tag{4}$$

$$E = c_v T + \frac{1}{2} V^2 \tag{5}$$

where the viscosity coefficient is assumed to be a constant, and the effect of the complex solid boundary on the flowfield is represented by body force $\mathbf{F}$. Because emphasis is placed on the inception period of flow instability, the flowfield is assumed to consist of mean flow and a small disturbance:

$$\mathbf{V} = \bar{\mathbf{V}} + v' \tag{6}$$

$$p = \bar{p} + p' \tag{7}$$

$$\rho = \bar{\rho} + \rho' \tag{8}$$

$$F = \bar{F} + F' \tag{9}$$

where $\bar{}$ represents the mean flow, and $'$ represents the flow disturbance. After Eqs. (6–9) are substituted into Eqs. (1–5), the linearized N–S equations are derived. The mean flow data can be computed by computational fluid simulation, which is generally used to solve 3-D steady RANS equations.

The body-force scalar is assumed to be a function of flowfield parameters:

$$F(\rho, p, \mathbf{V}) = \bar{F}(\bar{\rho}, \bar{p}, \bar{V}_r, \bar{V}_\theta, \bar{V}_z) + \frac{\partial F}{\partial \rho}\rho' + \frac{\partial F}{\partial p}p' + \frac{\partial F}{\partial V_r}v_r' + \frac{\partial F}{\partial V_\theta}v_\theta' + \frac{\partial F}{\partial V_z}v_z' \tag{10}$$

$$F' = \frac{\partial F}{\partial \rho}\rho' + \frac{\partial F}{\partial p}p' + \frac{\partial F}{\partial V_r}v_r' + \frac{\partial F}{\partial V_\theta}v_\theta' + \frac{\partial F}{\partial V_z}v_z' \tag{11}$$

Although the precise formula of the body force is not straightforward for some specific complicated flowfield, theoretically a body-force model can be used to reproduce the main effects of force source on the flowfield. It is noted that the body force produced by the complex configuration and solid boundary will definitely introduce great challenge to a general flow-stability problem during the process of establishing the eigenvalue equation. In 3-D CFD calculation, the body-fitted grid technique is generally implemented to cope with the twisty solid geometry. The complicated solid boundary increases the complexity of transforming linearized N–S equations from the physical domain to the computational domain. The immersed boundary (IB) method possibly provides an alternative way to model the complex solid boundary and was first designed by Peskin [26] to simulate blood-valve interaction. This method adopts a force term on the right side of the momentum equations to represent the effects of the solid boundary on the flowfield, and it is proved mathematically [27] that a material boundary effect on the flowfield is equivalent to a distribution force source. In the application of the IB method, the effects of immersed boundaries are represented as a singular force on the fluid. The interaction between boundaries and fluid is associated with the Dirac delta function.

Furthermore, the small perturbation of the flowfield is assumed to be in the form of harmonic decomposition:

$$\rho' = \tilde{\rho}(r, z)e^{i(-\omega t + m\theta)} \tag{12}$$

$$v_r' = \tilde{v}_r(r, z)e^{i(-\omega t + m\theta)} \tag{13}$$

$$v_\theta' = \tilde{v}_\theta(r, z)e^{i(-\omega t + m\theta)} \tag{14}$$

$$v_z' = \tilde{v}_z(r, z)e^{i(-\omega t + m\theta)} \tag{15}$$

$$p' = \tilde{p}(r, z)e^{i(-\omega t + m\theta)} \tag{16}$$

where $\sim$ represents the amplitude of flow perturbations.

After substituting Eqs. (12–16) into the linearized N–S equations, a second-order differential equation is derived:

$$\boldsymbol{A}\frac{\partial^2 \boldsymbol{\Phi}}{\partial r^2} + \boldsymbol{B}\frac{\partial^2 \boldsymbol{\Phi}}{\partial z^2} + \boldsymbol{Q}\frac{\partial^2 \boldsymbol{\Phi}}{\partial r \partial z} + \boldsymbol{C}\frac{\partial \boldsymbol{\Phi}}{\partial r} + \boldsymbol{D}\frac{\partial \boldsymbol{\Phi}}{\partial z} + \boldsymbol{G}\boldsymbol{\Phi} - i\omega \boldsymbol{H}\boldsymbol{\Phi} = 0 \tag{17}$$

$$\boldsymbol{\Phi} = \{\tilde{\rho}, \tilde{v}_r, \tilde{v}_\theta, \tilde{v}_z, \tilde{p}\}^T \tag{18}$$

and an eigenvalue equation can be expressed as follows:

$$\det[\boldsymbol{X}] = 0 \tag{19}$$

$$\boldsymbol{X} = \boldsymbol{A}D_{rr} + \boldsymbol{B}D_{zz} + \boldsymbol{Q}D_{rz} + \boldsymbol{C}D_r + \boldsymbol{D}D_z + \boldsymbol{G} - i\omega \boldsymbol{H} \tag{20}$$

$$D_{rr} \equiv \partial^2/\partial r^2, \qquad D_{zz} \equiv \partial^2/\partial z^2, \qquad D_{rz} = \partial^2/(\partial r \partial z), \qquad D_r \equiv \partial/\partial r, \qquad D_z \equiv \partial/\partial z \tag{21}$$

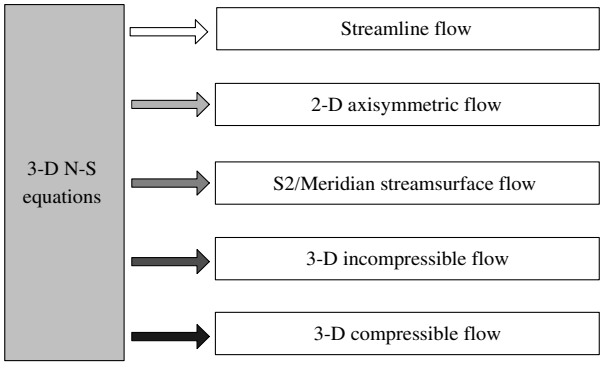

Fig. 1 Simplified calculation models of 3-D N–S equations.

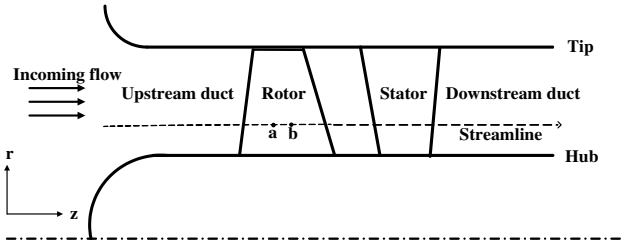

Fig. 2 Sketch map of one compressor stage in the meridian plane and two points on one streamline.

Then, the appropriate boundary condition for the specific flowfield is prescribed. After applying the coordinate transformation from the physical domain to the computational domain and using numerical discretization, Eq. (19) can be solved, and the imaginary part of the resultant complex eigenfrequency ω represents whether the system is stable with a negative value or unstable with a positive value. By applying the IB method, the numerical discretization can be performed straight on regular orthogonal grids rather than body-fitted grids. This would make the coordinate transformation possible for the complex configuration and flowfield.

Although the whole procedure of formulating the eigenvalue equation seems to be straightforward, Eq. (19) will be extremely difficult to be solved, which is caused by the constructing body force and the hugeness of the resultant eigenmatrix for a real 3-D viscous compressible flowfield with a complex solid boundary. Considering the specific flow-stability problem, several types of further simplification for calculating the flowfield, which is shown in Fig. 1, could be implemented to facilitate the solution of system stability.

In the following part of this paper, the presented general theory of flow stability is applied on the study of stall inception of the fan/compressors, which is one typical flow-instability problem. Cumpsty [28] outlined that, until recently, most satisfactory design systems of the fan/compressors are developed around a successful approach proposed by Wu [29] in which the flow is described by intersecting S1 and S2 stream surfaces in blade rows. To capture the main features of the rotating stall and to be accordance with the modern design methodology, the meridian average flowfield with the body force is studied in this work. Actually, the body-force model adopted in this study can be regarded as a particular application of the IB method in a simplified case. Additionally, the presented model herein can provide an alternative tool to check the overpredicted stall margin during the design phase of the fan/compressors.

III. Stall-Inception Model Based on the General Theory of Flow Stability

A single-stage fan/compressor system, which consists of an inlet duct, blade-rows region, inter-bladed row region, and an outlet duct, is shown in Fig. 2. In this paper, the circumferentially averaged flowfield and its derivative in the axial and radial directions are derived from steady CFD, which is performed by solving a routine 3-D RANS equations solver.

Then, a flow model for studying the stability of a small perturbation in a compressor flow needs to be developed. In this paper, the action of blades on the flowfield and the flow loss of kinetic energy caused by mixing and the shock wave outside the blade surface are represented by a body-force distribution, and the viscosity outside the blade surface is neglected. Much work (Adamczyk [30], Leboeuf and Trebinjac [31], Sturmayr and Hirsch [32], Chima [18], Gong et al. [20], etc.) has been published on the rational derivation of a flow model in a multistage turbomachine by using the blade-force approach. In the present model, the flowfield is described by 3-D, unsteady, compressible Euler equations with force source terms in the fixed frame of the coordinate system:

$$\frac{\partial \rho}{\partial t} + \frac{\partial (r\rho v_r)}{r\partial r} + \frac{\partial (\rho v_\theta)}{r\partial \theta} + \frac{\partial (\rho v_z)}{\partial z} = 0 \tag{22}$$

$$\frac{\partial v_r}{\partial t} + v_r \frac{\partial v_r}{\partial r} + v_\theta \frac{\partial v_r}{r\partial \theta} + v_z \frac{\partial v_r}{\partial z} - \frac{v_\theta v_\theta}{r} = -\frac{1}{\rho}\frac{\partial p}{\partial r} + F_r \tag{23}$$

$$\frac{\partial v_\theta}{\partial t} + v_r \frac{\partial v_\theta}{\partial r} + v_\theta \frac{\partial v_\theta}{r\partial \theta} + v_z \frac{\partial v_\theta}{\partial z} + \frac{v_\theta v_r}{r} = -\frac{1}{\rho}\frac{\partial p}{r\partial \theta} + F_\theta \tag{24}$$

$$\frac{\partial v_z}{\partial t} + v_r \frac{\partial v_z}{\partial r} + v_\theta \frac{\partial v_z}{r\partial \theta} + v_z \frac{\partial v_z}{\partial z} = -\frac{1}{\rho}\frac{\partial p}{\partial z} + F_z \tag{25}$$

$$\frac{\partial T}{\partial t} + v_r \frac{\partial T}{\partial r} + v_\theta \frac{\partial T}{r\partial \theta} + v_z \frac{\partial T}{\partial z} + \frac{R}{c_v} T \left(\frac{\partial (r v_r)}{r\partial r} + \frac{\partial v_\theta}{r\partial \theta} + \frac{\partial v_z}{\partial z} \right) = 0 \tag{26}$$

Theoretically, Eqs. (22–26) can be employed to study the stability of 3-D nonuniform flow in multistage compressors. In this work, we focus on computing the stall-inception point for a clean inlet condition, and the circumferential inlet distortion is out of consideration. The circumferential derivatives of mean flow in Eqs. (22–26) are assumed to be negligible. The rationality of this simplified flow model for multistage compressors will be made apparent during the model assessments. It is noted that the mean flow data can also be extracted from the meridian stream surface data, which are calculated by the streamline curvature method during the design stage of the fan/compressors.

A. Body-Force Model

To consider the effects of blades, flow mixing, and shock wave within the blade passages on the flowfield and to make the complicated problem computationally feasible, the body-force approach is taken to generate the physical sources of flow turning and loss. There is no unique mathematic model for the body-force term, and different sorts of body-force models developed by Longley [17], Chima [18], and Gong et al. [20] perform well in reproducing the flow detail in blade passages, provided that the conservation relations for mass, momentum, and energy are reflected correctly. The body-force model adopted in the present study is mainly on the basis of the work of Gordon [12] and Gong et al. [20], in which they made great progress on modeling the action of blades on flow, including the effects of the time-delay correlation and the spanwise distribution of pressure rise in the bladed region, respectively.

In the present work, a new body-force model F is proposed, which consists of three parts, as shown in Fig. 3. The first part represents F_v, which is normal to the mean camber line of the blades in the blade-to-blade surface and is designed to generate the flow deviation in the blade-to-blade direction. The second part is F_{t1}, which is assumed to generate the whole flow loss of kinetic energy within the blade passages. The last part is F_{t2}, which is parallel to the camber surface and streamline. F_{t2} is mainly caused by viscosity on the blade surface. Xu [33] conducted a rigorous study to assess viscous body forces for unsteady calculations and presented a simplified

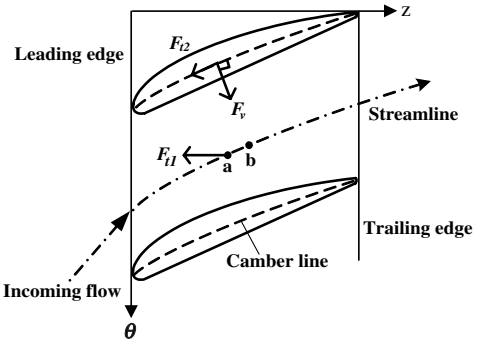

Fig. 3 Sketch map of the body force in the blade-to-blade surface and two points (a and b) on one streamline.

formulation to model the viscous force. The result verified that the viscous force is relatively small compared to the total blade forces. Therefore, F_{t2} is assumed to be negligible in this paper. The radial component of the total body force is assumed to be negligible due to the small radial inclination of the blades in this paper. Thus, F_{t1} is assumed to be an axial force. It is noted that the applicability of the following linearization process and this simplified body-force approach for reflecting the principle physical nature will be made apparent during the model assessment part.

After the flowfield of the fan/compressors is computed by 3-D steady numerical calculation, $F_{v\theta}$, which is the circumferential component of F_v, can be obtained:

$$F_{v\theta} = v_r \frac{\partial v_\theta}{\partial r} + v_z \frac{\partial v_\theta}{\partial z} + \frac{v_\theta v_r}{r} \tag{27}$$

In a steady, circumferentially averaged, two-dimensional (2-D) flowfield, $F_{v\theta}$ is formulated as

$$F_{v\theta} = v_z \frac{\partial v_\theta}{\partial z} \tag{28}$$

which is derived from the circumferential momentum equation. In accordance with Gordon's analysis [12], the local circumferential body force of blades is assumed to turn the relative flow toward the blade angle, i.e.,

$$F_{v\theta} = k_c v_z [v_z \tan\beta - (v_\theta - r\Omega) + \varepsilon] \tag{29}$$

The body force coefficient $k_c(r, z)$ is therefore determined by arranging Eqs. (27) and (29) as

$$k_c = \frac{v_r \frac{\partial v_\theta}{\partial r} + v_z \frac{\partial v_\theta}{\partial z} + \frac{v_\theta v_r}{r}}{v_z [v_z \tan\beta - (v_\theta - r\Omega) + \varepsilon]} \tag{30}$$

where ε is a parameter that is large enough to avoid the singularity of k due to the extreme small deviation angle of flow. Considering the orthogonality between F_v and the blade camber surface, its axial component can be derived directly:

$$F_{vz} = F_{v\theta} \tan\beta \tag{31}$$

The stagnation pressure and rotary stagnation pressure are defined as

$$p_t = p\left\{1 + \frac{\gamma - 1}{2} \cdot \frac{\rho[V_z^2 + V_r^2 + V_\theta^2]}{\gamma p}\right\}^{\frac{\gamma}{\gamma - 1}} \tag{32}$$

$$\bar{p}_t = p_t - \rho\Omega r v_\theta \tag{33}$$

Because of a variety of loss caused by mixing and viscosity in the flowfield of a fan/compressors system, the rotary stagnation pressure will decrease along the streamline. The flow loss of kinetic energy across the rotors and stators is assumed to be proportional to the local relative velocity magnitude. Assuming two points a and b lie on one streamline within the blade passage, the loss coefficient is derived as

$$\lambda = \frac{(\bar{p}_t)_b - (\bar{p}_t)_a}{\rho[v_z^2 + (v_\theta - \Omega r)^2]_a} \tag{34}$$

On the other hand, F_{t1} is designed to reproduce the effects of flow loss across the blade passages, and its distribution is derived by the following formula after the mean flow data are obtained by steady CFD:

$$F_{t1}\rho(z_b - z_a) = (\bar{p}_t)_b - (\bar{p}_t)_a \tag{35}$$

Therefore, F_t can be formulated as follows by manipulating Eqs. (34) and (35):

$$F_{t1} = \lambda \frac{[v_z^2 + (v_\theta - \Omega r)^2]}{(z_b - z_a)} \tag{36}$$

Finally, the axial component of body force is given by Eqs. (31) and (36):

$$F_z = F_{vz} + F_{t1} \tag{37}$$

and the circumferential component of the body force is given by Eq. (29):

$$F_\theta = F_{v\theta} \tag{38}$$

In accordance with Gordon's analysis [12], the unsteady action of blades on the flowfield is described by the body-force function, which responds to the local unsteady 3-D flow variations in the blade region, and the unsteady force disturbances f_θ and f_z are modeled by a first-order lag equation with a time-delay constant τ. The linearized form of the body force is formulated as

$$(1 - i\omega\tau + im\Omega\tau) f_\theta = \frac{\partial F_\theta}{\partial v_\theta} v_\theta' + \frac{\partial F_\theta}{\partial v_z} v_z' \tag{39}$$

$$(1 - i\omega\tau + im\Omega\tau) f_z = \frac{\partial F_z}{\partial v_\theta} v_\theta' + \frac{\partial F_z}{\partial v_z} v_z' \tag{40}$$

The time-delay constant τ, which represents the lag between the output response and input data, is employed to describe the unsteady performance of the fan/compressors. The time scale of τ is generally assumed to be of the order of flow-through time in the bladed region. Parameter studies on this constant are conducted in the following model assessments.

B. Establishment of Eigenvalue Problem

Because emphasis is placed on the inception condition of rotating stall in this investigation, the flow perturbation is assumed to be small, and the solutions are in accordance with Eqs. (12–16). He [15] verified that the first circumferential mode had the most destabilizing effect. Gordon [12] also demonstrated that higher-order modes were usually more stable than lower-order modes unless extreme stage mismatching and severe inlet distortion occur. Emphasis in this paper is therefore placed on the lowest-order circumferential and radial mode that dominates the stability of the fan/compressors system.

The boundaries are prescribed such that there are no inlet disturbances coming from outside the system at the upstream end of the duct and no reflection at the downstream end of the duct, and the slip condition is used at the hub and the tip of the annular duct. After substituting Eqs. (12–16) and Eqs. (39) and (40) into Eqs. (22–26), the linearized governing equations are derived as

$$(\boldsymbol{C}D_r + \boldsymbol{D}D_z + \boldsymbol{G} - i\omega\boldsymbol{H})\boldsymbol{\Phi} = 0 \tag{41}$$

where $\boldsymbol{C}$ is a radial derivative matrix, and $\boldsymbol{D}$ is an axial derivative matrix. The second-order partial derivatives disappear because

viscosity is neglected in this simplified model. Because Eq. (41) is homogeneous, a nontrivial solution of $\boldsymbol{\Phi}$ exists only if the determinant of the coefficients matrix is zero, i.e.,

$$\det[\boldsymbol{X}] = 0 \tag{42}$$

$$\boldsymbol{X} = \boldsymbol{C}D_r + \boldsymbol{D}D_z + \boldsymbol{G} - i\omega\boldsymbol{H} \tag{43}$$

Solving the established eigenvalue problem of Eq. (41) or (42) leads to the resultant complex frequency $\omega = \omega_r + i\omega_i$, the imaginary part of which represents whether the system is stable with a negative value or unstable with a positive value, and the real part of which determines the rotating frequency of the precursor wave. Two nondimensional factors are defined as relative speed (RS) and damping factor (DF):

$$RS = \frac{\omega_r}{2m\pi} \cdot \frac{60}{\Omega} \tag{44}$$

$$\mathrm{DF} = \frac{r_t \omega_i}{mU_0} \tag{45}$$

IV. Numerical Method for Solving the Stability Equation

After establishing an eigenvalue equation for the fan/compressors flow-instability inception, solving the most unstable mode of Eq. (42) is still a tricky problem. To facilitate its solution, the equation is discretized over the computational grid, and the numerical method is given in this part.

A. Numerical Discretization

To improve the accuracy of the numerical solution and to decrease the discrete points for saving computation cost, the spectral technique based on Chebyshev–Gauss–Lobatto points is implemented, which is adopted widely in the boundary-value problem. The physical grids in the (z, r) plane are transformed into a computational plane (ζ, η) so that the transformed grid lines are orthogonal and suitable for the spectrum method. The eigenvalue of Eq. (42) is solved numerically over the spectral grids that satisfy

$$\xi_i = \cos(\pi i/N_r);\ i = 0, 1, \ldots, N_r \tag{46}$$

$$\eta_j = \cos(\pi j/N_z);\ j = 0, 1, \ldots, N_z \tag{47}$$

where N_r and N_z are the total number of nodes in each subdomain in the ζ and η coordinates. Assuming that $f(\zeta)$ is a smooth function of ζ on the interval $[-1, \quad 1]$, $f(\zeta)$ is interpolated by constructing an N-order interpolation polynomial $g_j(\zeta)$:

$$f(\xi) = \sum_{j-0}^{N} f(\xi_j) g_j(\xi) \tag{48}$$

$$g_j(\xi) = \frac{(-1)^{j+1}(1-\xi^2)T'_N(\xi)}{c_j N^2(\xi - \xi_j)}\ i = 0, 1, \ldots, N \tag{49}$$

where $T_N(\zeta)$ is an N-order Chebyshev polynomial in the form of

$$T_N(\xi) = \cos(N \cos^{-1} \xi) \tag{50}$$

and its derivative is

$$T'_N(\xi) = \frac{N \cdot \sin(N \arccos\ \xi)}{\sqrt{1-\xi^2}} \tag{51}$$

and the coefficient c_j is formulated as

$$c_j = \begin{cases} 2, j = 0, N \\ 1, 0 < j < N \end{cases} \tag{52}$$

The derivative of $f(\zeta)$ at the collocation points satisfies

$$\frac{\mathrm{d}f(\xi_i)}{\mathrm{d}\xi} = \sum_{j=0}^{N} D_{ij} f(\xi_j) i = 0, 1, \ldots, N \tag{53}$$

where the derivative matrix D_{ij} is formulated by Don and Solomonoff [34] as

$$D_{ij} = \begin{cases} \frac{c_i(-1)^{i+j}}{2c_j \sin\frac{\pi}{2N}(i+j)\sin\frac{\pi}{2N}(-i+j)} & i \neq j;\ i = 0, \cdots, \frac{N}{2};\ j = 0, \cdots, N \\ \frac{-\cos(\frac{\pi i}{N})}{2\sin^2(\frac{\pi}{N}i)} & i = j;\ i = 1, \cdots, \frac{N}{2};\ j = 1, \cdots, N \\ \frac{2N^2+1}{6} & i = j = 0 \\ -D_{N-i,N-j} & i = \frac{N}{2}+1, \cdots, N;\ j = 0, \cdots, N \end{cases} \tag{54}$$

Singularity generally appears on the leading edge of the airfoil with unsteady flow. In general, any accurate computation of airfoil flow requires a special treatment on singularities. For an isolated airfoil, Rusak and Morris [25] and Rusak [35] treated the nose singularity for subsonic and transonic flow by using matched asymptotic methods of inner solution around the airfoil nose and the outer region described by the small disturbance solution, whereas for the cascade case, Namba [36] used a type of mathematical treatment to deal with the singularity on the leading and trailing edges of the compressor blade. In the present work, the body-force model is applied to consider the main effects of cascade on the flowfield without more flow details, especially on both leading and trailing edges of the blades. On one hand, such simplification has resulted in a reasonable eigenvalue stability model with high computation efficiency; on the other hand, there is no doubt that flow details on the blades should be studied in future work for more accurate computation results. In this paper, the domain decomposition method is applied to deal with the singularity of the body force due to no body force in the blade-free region. Some transmission conditions are taken into account at the interfaces between subdomains. The continuity conditions at the interface $\zeta 1\_2$ between subdomain 1 and subdomain 2 are

$$f_1(\xi_{12}) = f_2(\xi_{12}) \tag{55}$$

$$\frac{\mathrm{d}f_1(\xi_{12})}{\mathrm{d}\xi} = \frac{\mathrm{d}f_2(\xi_{12})}{\mathrm{d}\xi} \tag{56}$$

B. Numerical Solution

In Eq. (42), the column vector $\boldsymbol{\Phi}$ of the perturbation amplitudes has $K = 5N_r \cdot (N_{zf} + N_{zb})$ entries, where N_r is the total number of radial nodes, and N_{zf} and N_{zb} are the total number of axial nodes in the blade-free and blade-row regions, respectively. The $K \times K$ matrix $\boldsymbol{X}$ is very large for a modest number of grid nodes. For instance, there are 20 radial nodes and 90 axial nodes, which are spaced 20 upstream, 20 downstream, 20 in the rotor, 20 in the stator, and 10 in the interbladed row region in a typical one-stage compressor (i.e., $K = 9000$). The matrix $\boldsymbol{X}$ contains 81 million complex value entries. It is found that matrix $\boldsymbol{X}$ will become extremely huge for multistage fan/compressors, which will make the solution of the eigenvalue equation a very tough problem. In fact, because of the numerical rounding error, it is not feasible to determine the eigenfrequency for which the determinant of $\boldsymbol{X}$ is zero. Solving Eq. (42) is also not possible using the traditional QR decomposition method because of the lack of accuracy. Such a difficulty exists in various flow-stability problems, and much research work has been conducted previously. The Newton–Raphson iteration method is widely used to solve such an eigenvalue equation. However, there is

no general rule available to determine its physical solution. Malik [37] implemented an inverse iteration technique to solve the eigenvalue, and this method is very sensitive to the initial estimate of ω, and much empiricism is required to identify pseudomodes. Sun et al. [14] extended the winding number integral approach to solve the matrix equations for a rotating stall. The essence of this approach is a smart application of the argument principle and Nyquist stability criterion [38,39]. Nevertheless, it is not feasible for the present problem because of the inevitable and unsustainable computation consumption required for a series of determinant calculation.

In this paper, SVD is adopted over fine grids on the complex plane to find the solution of Eq. (42). Actually, this approach was adopted in much study [40,41] on searching the roots for which a matrix with many entries becomes singular. As described by Woodley and Peake [40], SVD is a very powerful technique for dealing with matrices that are either singular or numerically very close to singular. This technique is based on the theorem of linear algebra that any $M \times N$ matrix $\boldsymbol{X}$ can be factorized into a product of one $M \times N$ column-orthogonal matrix $\boldsymbol{U}$, one $N \times N$ diagonal matrix $\boldsymbol{W}$ with positive or zero elements (the singular values), and the transpose of one $N \times N$ orthogonal matrix $\boldsymbol{V}$ (More details regarding the SVD method are given by Press et al. [42].):

$$(\boldsymbol{X}) = (\boldsymbol{U}) \cdot \begin{pmatrix} \omega_1 & & \\ & \ddots & \\ & & \omega_N \end{pmatrix} \cdot (\boldsymbol{V}^T) \tag{57}$$

The condition number of a matrix is formally defined as the ratio of the largest and smallest singular values. Strictly speaking, a matrix is singular as long as the condition number is infinite, and the determinant of a matrix is zero if only the reciprocal of the condition number is zero. However, due to the rounding error accumulated during the numerical process, it is often unlikely to approach the machine's floating-point precision. In accordance with the Cooper et al. [41], the authors therefore define the roots of the eigenvalue equation as occurring when the reciprocal of the condition number is significantly smaller than elsewhere.

V. Model Validation and Comparisons with Experimental Results

In this part, four assessments are performed to validate the ability of the present model to calculate the stall-onset point, and some discussions are given. The first assessment demonstrates the prediction accuracy by comparing the resultant unstable mode with the experimental data of a low-speed compressor. A simplified version of this model is developed in the second assessment, which is established on a one-dimensional streamline. Comparisons with the 3-D model are conducted to reveal the nonnegligible effects of spanwise distribution of the flowfield on stall margin. The last two assessments are to check the applicability of this model on predicting the stall-onset point of a transonic single rotor at low and high rotational speed.

A. Numerical Prediction and Comparisons with Experimental Results of a Low-Speed Compressor

Nie et al. [43] experimentally studied micro air injection for stall margin enhancement on a low-speed three-stage axial-flow compressor rig at the Institute of Engineering Thermophysics at the Chinese Academy of Sciences, and the spike-type stalling process is verified by wavelet analysis. This compressor rig has three identical stages. Tong [44] carried out an experimental study to explore the mechanism of stall suppression by micro-injection on a single-rotor system, which includes only the first rotor of this rig. Its main design specifications are given by Nie et al. [43], and the design mass flow is 2.6 kg/s at 2400 rpm with a tip clearance of 2.8% of tip chord. A side view and schematic can be seen in Fig. 4. Figure 5 shows the measurement system with single rotor and motor labeled as 1 and 2, inverter labeled as 3, static pressure taps and 3-hole probe labeled as 4 and 5, transducers labeled as 6 and 7, steady sensor box labeled as 8,

Fig. 4 Side view of the single-rotor test rig (courtesy of Nie et al. [43]).

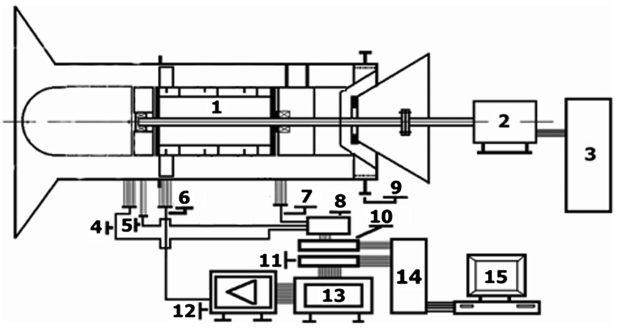

1. Single rotor 2. Motor 3. Inverter (IPF-18.5) 4. Static pressure taps 5. 3-hole probe 6. Transducers (XCS-190) 7. Transducers (XCS-190) 8 Steady sensor box 9. Cone valve 10. BNC Connectors (BNC-2090) 11. BNC Connectors (BNC-2090) 12. Amplifiers (8300AU) 13. Data recorder (XR-700) 14. Data acquisition board (PCI-6071E) 15. Computer

Fig. 5 Schematic of the compressor rig and measurement system (courtesy of Tong [44]).

cone valve labeled as 9, BNC Connectors labeled as 10 and 11, amplifiers labeled as 12, data recorder and data acquisition board labeled as 13 and 14, and computer labeled as 15. Model assessment in this section is made on this single rotor.

To validate the present flow-instability inception model, a dynamic experiment is performed with emphasis on the stalling process and eight on-shroud pressure transducers in front of the rotor are installed to record the static pressure oscillation. Figure 6 shows that a form of short scale pips was observed just before stall in the time revolution of the static pressure signal. After the pips propagated circumferentially

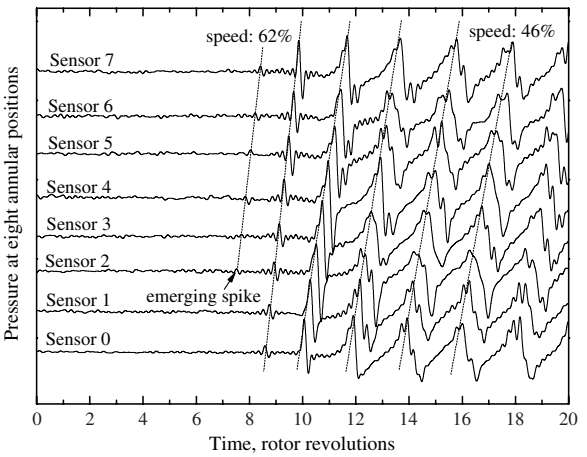

Fig. 6 Time evolution of the static pressure near the shroud in front of the rotor.

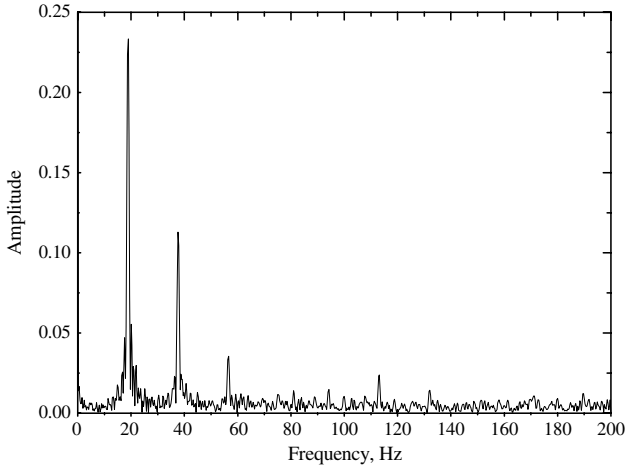

Fig. 7 Pressure spectra in the frequency domain after stall.

at 62% rotor speed, the spike-type disturbance triggers the stall. The final stall cells evolved in less than five rotor revolutions and rotated at 46% rotor speed. A pressure spectrum in frequency domain after stall is shown in Fig. 7. The final instability frequency is located on an interval of 16 and 20 Hz, i.e., 40–50% rotational frequency of the rotor, which is assumed to be the most unstable eigenfrequency of this rotor.

The steady 3-D viscous compressible flowfield is computed on a total number of approximately 746,000 grid nodes with a tip clearance block for one single blade passage of this single rotor. The grid has 105 points axially, 41 points circumferentially, and 41 points spanwise. The solution algorithm is based on central discretization and a four-stage Runge–Kutta scheme coupled with the Spalart–Allmaras turbulence model, multigrid, and local time-stepping technique for convergence.

Figure 8 compares the static pressure rise between the CFD calculation and experimental results, and the efficiency is not measured. The calculated pressure rise is a reasonable approximation to the experimental data, especially nearby the design point. It is found that the mass flow just before the numerical stall condition is 1.995 kg/s, whereas the mass flow at the measured stall point is 2.309 kg/s. The relative error is about 13.6%, and the stall margin is overpredicted by 12.1%. Obviously, as an unsteady process, rotating stall could not be estimated roughly by the numerical convergence of the steady flow simulation.

The calculated mean flow data on meridian plane are processed as polynomial fits of axial and radial coordinates to eliminate the nonsignificant eigenfrequency due to the local vortex. After introducing the flowfield data into the present model, the complex eigenvalues of the compressor system accompanying the throttling process are computed, which are displayed in Fig. 9. Nine

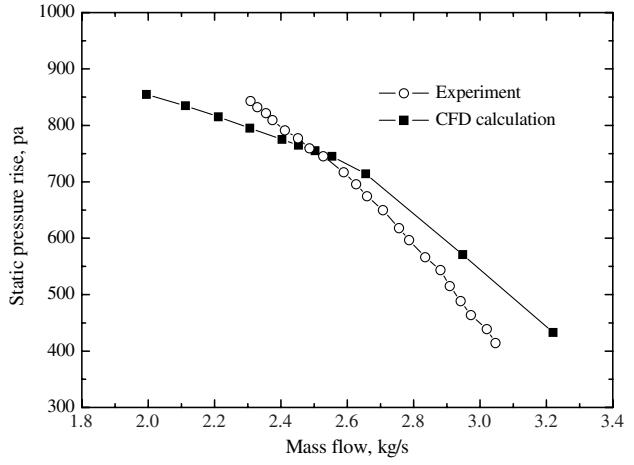

Fig. 8 Static pressure rise of the low-speed single rotor.

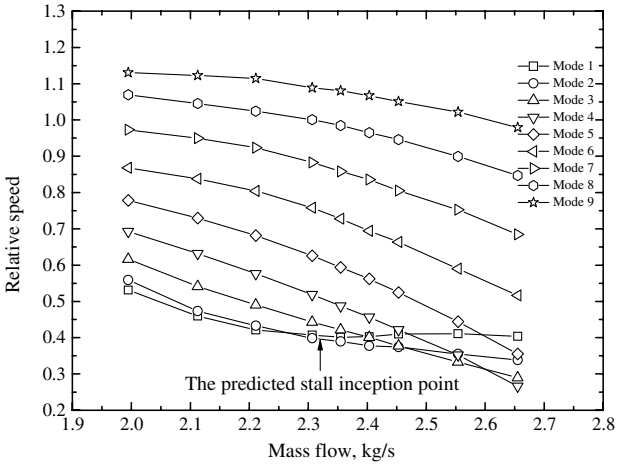

a)

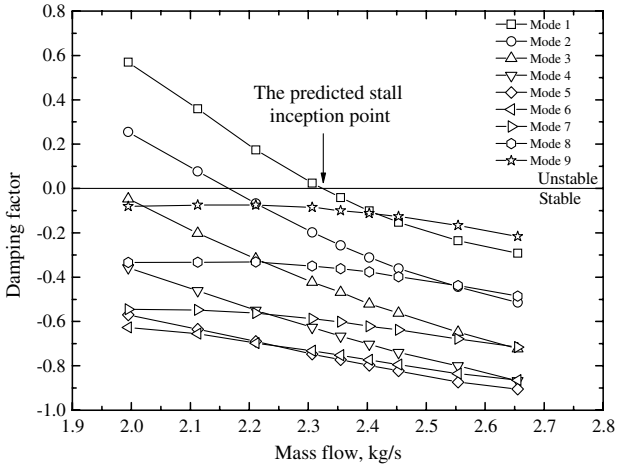

b)

Fig. 9 Computed eigenvalues of the low-speed rotor: a) relative speed, and b) damping factor.

eigenmodes within the selected solution interval are obtained for every operation point, which are sequenced as modes 1 to 9 according to the magnitude of the real part. In this assessment, several different values of the time-delay constant are tested, and no visible change of eigenvalue emerges.

It is found that the DFs of all nine modes increase gradually as the rotor approaches flow instability. The first five modes, which propagate slowly, approach instability faster than the last four modes, which propagate rapidly. The DF of mode 1 changes first from negative to positive at a value of mass flow equal to 2.324 kg/s. The sign change of the DF represents the imminent instability. The relative error of the mass flow between the predicted stall-inception point and the measured instability point is 0.65%. Although the throttling continues, the RSs of all the modes increase, with an exception of slight decrease for mode 1 before stall. The propagation speed of this most unstable mode at stall inception is 40.5% rotational frequency, which is within the measured dominant instability frequency interval. The comparison between computed results with experimental data at the stall-onset point and instability frequency validates the prediction accuracy of the proposed flow inception model, and it makes the capacity of adopting this model for a spike-type stalling process apparent.

B. Comparisons with a Further Simplified Version of the Proposed Model

Most 2-D stability models (for example, Nenni and Ludwig [9], Stenning [45]) analyze the spanwise average of flow nonuniformity, and the radial distribution of the flowfield is neglected. We will show in this assessment that a low-dimensional model has a lack of

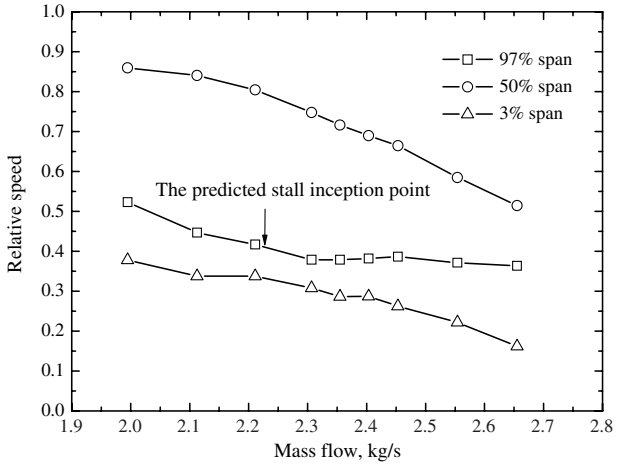

a)

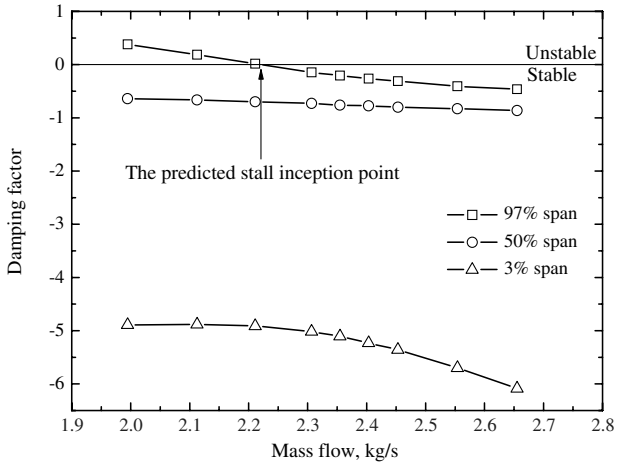

b)

Fig. 10 Computed eigenvalues by the simplified model for the low-speed compressor: a) relative speed, and b) damping factor.

accuracy when it is compared with a 3-D stall-inception model. In this section, a streamline model of stall inception is developed, which is based on the same theory presented in Sec. IV. The only two differences between these two models exist on the governing equations and the dimensionality of the matrix involved in the eigenvalue equation. Details of how the simplified version of the present model is established are given in the appendix.

Figure 10 shows the computed result using the simplified model on three different streamlines at 97%, 50%, and 3% span. The DFs of all the three modes increase as the mass flow is throttled, and it first crosses the critical line on the 97% span streamline at 2.225 kg/s, which is the predicted stall-inception point. It is indicated that the relative error between this point and the measured instability point is −3.63%. This simplified low-dimensional model overpredicts the stall margin. Tong [44] conducted wavelet analysis on the pressure signals and experimentally observed that flow separation and stall precursor first emerge at the tip region of this rotor. It is indicated that this simplified model successfully predicts the most unstable region, but the prediction accuracy of the stall-inception point is obviously less accurate than the 3-D model. Through the whole throttling process, the RSs of all three modes increase, with an exception of a slight decrease for 97% span before stall, and the propagation speed at stall inception is 40.5% design rotational frequency. These features are in accordance with the 3-D model prediction. However, the computed frequency spectrum using this simplified mode is not as broad as the 3-D model. In addition, the eigenmode propagates faster at 50% span than at 97% and 3% span. In conclusion, this assessment case validates the advantage of the 3-D model over the low-dimensional model. The whole spanwise flow distribution should be considered to get a more accurate stall margin prediction.

C. Eigenvalues of High Subsonic Compressor Flow-Instability Inception

In this section, the stall-inception eigenvalues of a transonic compressor are computed based on a typical example (i.e., NASA Rotor 37). The purpose of this calculation is to test the prediction ability of the model for high subsonic compressor flow. Thus, the mean flowfield data at 60% design rotational speed is used as the input parameters, and the spanwise distribution of the inlet relative Mach number ranges from 0.6 to 0.9. The details of the configuration and characteristics of this rotor were given in [46], and the detailed experimental data were provided by Suder [47].

The procedure for the steady flowfield solution of Rotor 37 is in accordance with Sec. V.A. Because the configuration is more complex than the low-speed single rotor, the total of grid points is approximately 750,000, which is sufficient to get a grid-independent solution. Figure 11 shows a comparison of characteristics between steady RANS calculation and experimental data. The calculated trends are in accordance with experimental data with underpredicted pressure ratio by 2.5% and efficiency by 3% before stall.

It is shown that the mass flow at the computational convergence point is about 9.68 kg/s, which is much lower than 10.56 kg/s at the measured stall-inception point. The relative error is 8.3% (i.e., the stall margin is overpredicted by about 8.0%).

After introducing the mean flow data on the meridian plane into the present stall-inception model, the resultant eigenfrequency at several different operation conditions along the characteristics line is displayed in Fig. 12. Six eigenmodes within the selected solution interval are computed for each operation point of Rotor 37, which are sequenced as modes 1 to 6 according to the magnitude of the imaginary part.

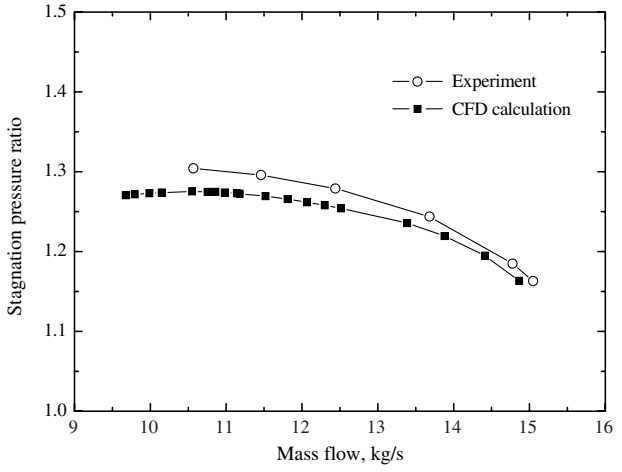

a)

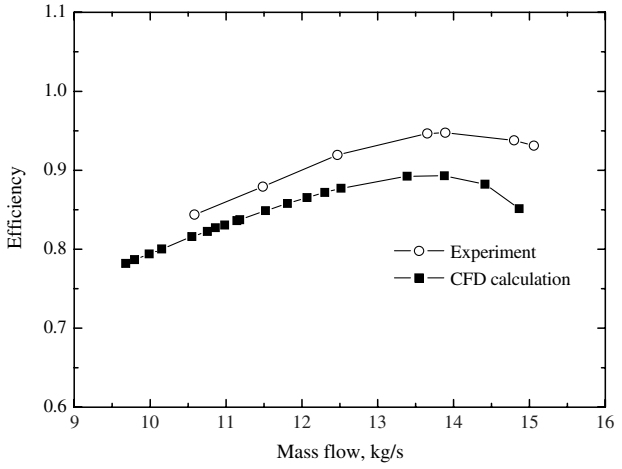

b)

Fig. 11 Characteristics of NASA Rotor 37 at 60% design rotational speed: a) stagnation pressure ratio, and b) efficiency.

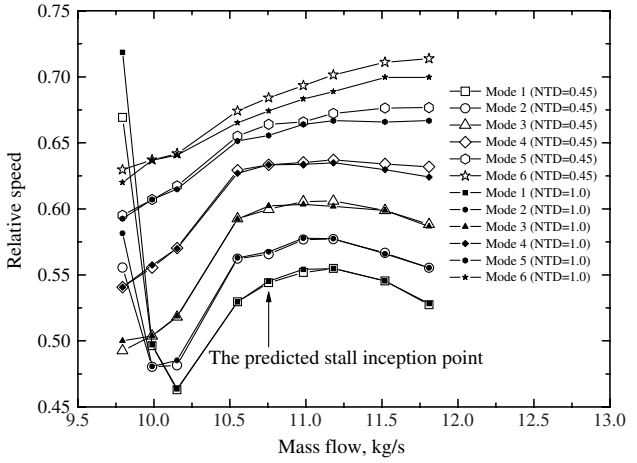

a)

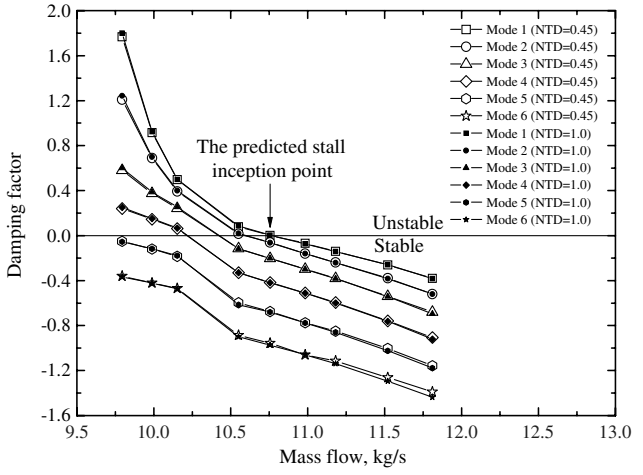

b)

Fig. 12 Computed eigenvalues of NASA Rotor 37 at 60% design rotational speed: a) relative speed, and b) damping factor.

In this paper, the nondimensional time delay (NTD) is defined as the time-delay constant τ divided by the flow-through time within the bladed region. In some studies before, it seems that NTD affects the accuracy of the instability prediction, and there is not yet a unified principle to determine its value. Hoying et al. [48] rigorously tested the effects of this constant on stall-inception prediction. He suggested that two values of NTD equal to 0.45 for loss and 1.0 for turning of the bladed region flow yield the best agreement with data in his paper. Haynes [49] compared the measured dynamics of one compressor with predictions given by a stability model, and a value of NTD equal to 1.5 was found to perform well. In this paper, Parameter study on time-delay constant is conducted for two values of NTD equal to 0.45 and 1.0. The results indicate that the proposed model is not strongly sensitive to this constant apart from slightly difference occurring far away the stall point.

It is shown that the RS before the computed stall point ranges between 0.50 and 0.75, which is in accordance with the measured propagation speed of stall precursor observed in many experiments. As the throttling progressively continues, the RS of the first unstable mode (mode 1) decreases visibly from 11.2 kg/s and remarkably, nearby the stall-inception point, an analogous phenomenon is also observed in many experimental studies. On the other hand, the DFs of all six modes increase linearly as the flowfield approaches instability. The DF of mode 1 first crosses the critical line when the mass flow decreases to 10.75 kg/s. This computed stall-inception point is quite close to the measured stall point, and the relative error is less than 1.8%. The propagation speed of the most unstable mode at computed stall-onset point is 54.4% of the design rotational frequency. After crossing the critical line of the system's stability, the DFs of modes 1 and 2 rise rapidly. The occurrence of this nonlinear development may be related to the nonlinear feature of the poststall process of the fan/compressors system. Although this correlation is a conjecture, the most unstable mode predicted by this linear model possibly provides an appropriate initial disturbance for the initial boundary-value problem, which aims to study the nonlinear development of stall precursor.

In conclusion, this assessment validates the ability of this model to predict the stall-onset point for a high-speed compressor at a low rotational speed. It is noted that the prediction was conducted on 10 CPU nodes for 11 h, which obviously is a sustainable computation cost for an industrial application.

D. Eigenvalues of Transonic Compressor Flow-Instability Inception

As far as the authors know, little research was conducted on stall-inception prediction of transonic flow with a general compressor configuration. The shock wave embedded in cascade passages, which plays a vital role in the flowfield, introduces great difficulty in modeling the compressor system. However, the strong discontinuity brought on by the shock wave is eliminated in the meridian average flowfield. The last model assessment, which is conducted on a NASA Rotor 37 at design rotational speed, is to exploit the potential of predicting the instability inception of transonic flow for the first time. The maximum relative Mach number at the tip of this rotor is greater than 1.4.

Figure 13 shows a comparison between steady RANS calculation and experimental data of Rotor 37. The calculated characteristics trend is in accordance with experimental data with the underpredicted

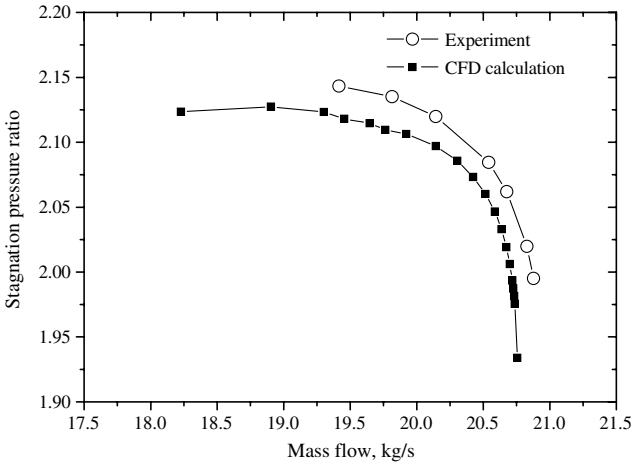

a)

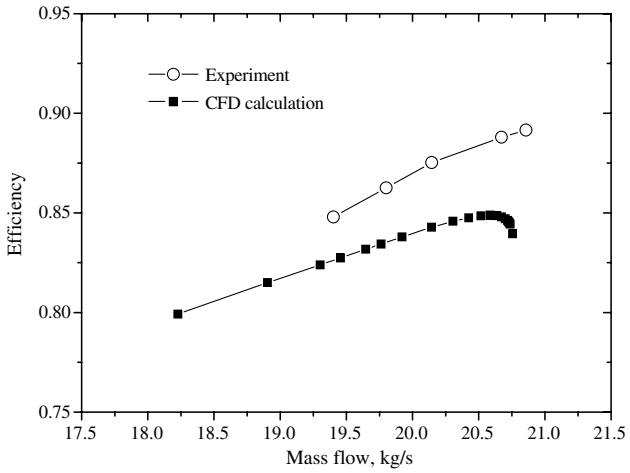

b)

Fig. 13 Characteristics of NASA Rotor 37 at design rotational speed: a) stagnation pressure ratio, and b) efficiency.

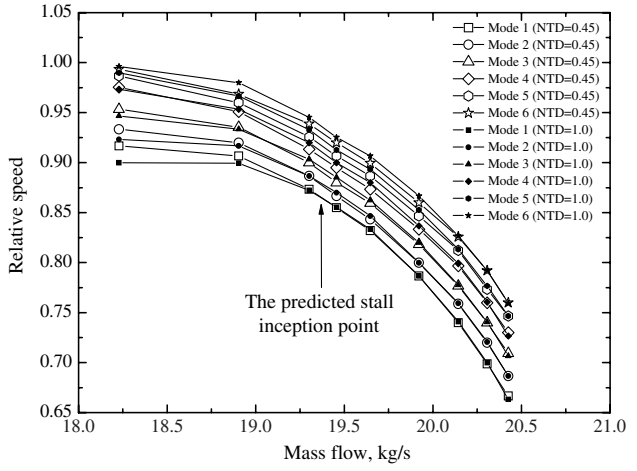

a)

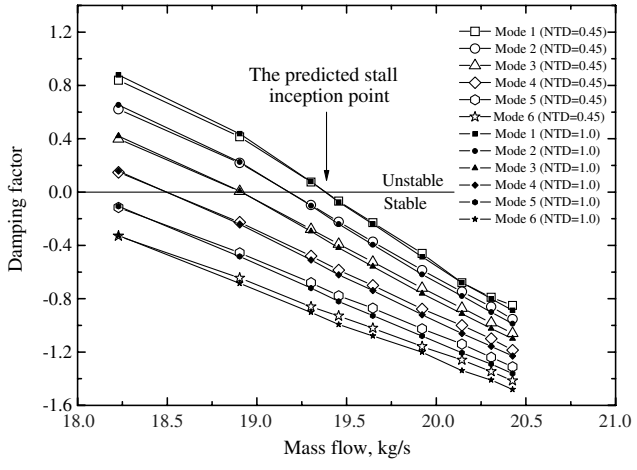

b)

Fig. 14 Computed eigenvalues of NASA Rotor 37 at design rotational speed: a) relative speed, and b) damping factor.

stagnation pressure ratio by 1.5% and efficiency by 3.5% before stall. It is found that the mass flow at the computational convergence point is approximate 18.2 kg/s, and the experimental stall-inception point is at 19.4 kg/s. The relative error is 6.19%.

Six eigenmodes within the selected solution interval are computed for each operation point of Rotor 37 along the characteristics line. These resultant eigenvalues, which are displayed in Fig. 14, are sequenced as modes 1 to 5 according to the magnitude of the imaginary part. It is shown that all the RS and DFs increase progressively as the mass flow is throttled. The most unstable mode (mode 1) first passes through the neutral line at 19.37 kg/s, which is the computed flow-instability inception point. The corresponding propagation speed is 86.5% of the rotational speed of the rotor. The relative error between the computed and measured stall-inception points is less than 0.16%. As the throttling continues, all the modes approach instability in order. It is indicated once again that two NTD (0.45 and 1.0) result in minor difference of the resultant eigenvalue. This assessment validates the capacity of the proposed theory on computing the eigenvalue of the transonic flow.

VI. Conclusions

A general theory of flow-instability inception in turbomachinery is proposed in this paper, and its application on three-dimensional (3-D) compressible stall onset is developed for a multistage fan/compressors system. The ability of the present model to predict the stall-inception point is validated against experimental data of both low and high-speed rotors. Four conclusions are deduced as follows.

1) This model is capable of predicting the stall-onset point of subsonic and transonic flows with a reasonable accuracy, and it is sustainable in terms of computation consumption for industrial application. Especially, the predicted results compared with the measured data for the present four assessments have a relative error of less than 1.8%.

2) Although the simplified streamline model can predict the location and propagation speed of the most unstable mode with an approximate accuracy as a 3-D stall-inception model, the stall margin is overpredicted in this paper. It is revealed that the effects of the flow spanwise distribution on the stall margin are nonnegligible, and the presented results validate the necessity of a 3-D flow-stability model for getting a more accurate stall margin prediction.

3) The resultant unstable mode of the fan/compressors system possibly provides an appropriate initial disturbance for further research on the nonlinear evolution of stall precursor. Future work is required to verify this viewpoint.

4) This model can provide an unambiguous judgment on stall inception without numerous requirements of empirical relations of loss and deviation angle. It could be employed to check an overpredicted stall margin during the design phase of new fan/compressors.

Appendix A: Simplified Version of the Present Stall-Inception Model

A 2-D flow-stability model, which is the simplified version of the 3-D stall-inception model, is presented herein. This model is established on one arbitrary hypothetical streamline in a multistage fan/compressors system, which is displayed in Fig. A1. The only two differences between the simplified version and the origin model exist on the governing equations and the dimensionality of matrix involved in the eigenvalue equation. The flowfield is described by 2-D, unsteady, compressible Euler equations with force source terms in a streamline coordinate system:

$$\frac{\partial \rho}{\partial t} + v_s \frac{\partial \rho}{\partial s} + v_\theta \frac{\partial \rho}{r\partial \theta} + \rho \frac{\partial v_s}{\partial s} + \rho \frac{\partial v_\theta}{r\partial \theta} = 0 \tag{A1}$$

$$\frac{\partial v_s}{\partial t} + v_s \frac{\partial v_s}{\partial s} + v_\theta \frac{\partial v_s}{r\partial \theta} - \frac{v_\theta^2}{r}\frac{\partial r}{\partial s} = -\frac{1}{\rho}\frac{\partial p}{\partial s} + F_s \tag{A2}$$

$$\frac{\partial v_\theta}{\partial t} + v_s \frac{\partial v_\theta}{\partial s} + v_\theta \frac{\partial v_\theta}{r\partial \theta} + \frac{v_s v_\theta}{r}\frac{\partial r}{\partial s} = -\frac{1}{\rho}\frac{\partial p}{r\partial \theta} + F_\theta \tag{A3}$$

$$\frac{\partial T}{\partial t} + v_s \frac{\partial T}{\partial s} + v_\theta \frac{\partial T}{r\partial \theta} + \frac{R}{c_v} T\left(\frac{\partial v_s}{\partial s} + \frac{\partial v_\theta}{r\partial \theta}\right) = 0 \tag{A4}$$

The flow velocity is assumed to be along the streamline, and the curvature variation of streamline is considered in this simplified model. In accordance with the developed 3-D stall-inception model, an eigenvalue equation is established analogously with the homologous body-force model:

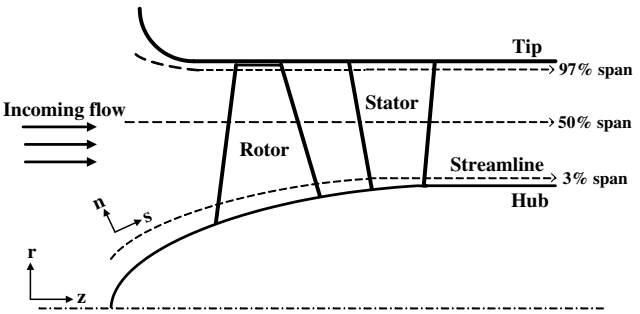

Fig. A1 Sketch map of a compressor stage in the meridian plane and one arbitrary streamline.

$$\det[\boldsymbol{X}] = 0 \tag{A5}$$

$$\boldsymbol{X} = \boldsymbol{C}\boldsymbol{D}_s + \boldsymbol{G} - i\omega\boldsymbol{H} \tag{A6}$$

The resultant matrix $\boldsymbol{X}$ involved in Eq. (A5) has $4N_r \cdot (N_{zf} + N_{zb})$ entries, rather than $5N_r \cdot (N_{zf} + N_{zb})$, where N_r is the number of spanwise nodes, and N_{zf} and N_{zb} are the total number of axial nodes in the blade-free and blade-row regions.

Acknowledgments

The authors would like to thank Nie Chaoqun and Tong Zhiting for providing experimental data. This work is supported by the 973 Program (grant 2012CB720200) and the National Science Foundation of China (grants 51076006, 50736007, and 50890181).

References

[1] Greitzer, E. M., "Surge and Rotating Stall in Axial Flow Compressors: Part 1 and Part 2," *Journal of Engineering for Power*, Vol. 98, No. 2, 1976, pp. 190–217. doi:10.1115/1.3446138

[2] Garnier, V. H., Epstein, A. H., and Greitzer, E. M., "Rotating Waves as a Stall Inception Indication in Axial Compressors," *Journal of Turbomachinery*, Vol. 113, No. 2, 1991, pp. 290–302. doi:10.1115/1.2929105

[3] McDougall, N. M., Cumpsty, N. A., and Hynes, T. P., "Stall Inception in Axial Compressors," *Journal of Turbomachinery*, Vol. 112, No. 1, 1990, pp. 116–125. doi:10.1115/1.2927406

[4] Day, I. J., "Stall Inception in Axial Flow Compressors," *Journal of Turbomachinery*, Vol. 115, No. 1, 1993, pp. 1–9. doi:10.1115/1.2929209

[5] Camp, T. R., and Day, I. J., "A Study of Spike and Modal Stall Phenomena in a Low-Speed Axial Compressor," *Journal of Turbomachinery*, Vol. 120, No. 3, 1998, pp. 393–401. doi:10.1115/1.2841730

[6] Day, I. J., Breuer, T., Escuret, J., Cherrett, M., and Wilson, A., "Stall Inception and the Prospects for Active Control in Four High-Speed Compressors," *Journal of Turbomachinery*, Vol. 121, No. 1, 1999, pp. 18–27. doi:10.1115/1.2841229

[7] Wilson, A. G., and Freeman, C., "Stall Inception and Development in an Axial Flow Aeroengine," *Journal of Turbomachinery*, Vol. 116, No. 2, 1994, pp. 216–225. doi:10.1115/1.2928356

[8] Tryfonidis, M., Etchevers, O., Paduano, J. D., Epstein, A. H., and Hendricks, G. J., "Prestall Behavior of Several High-Speed Compressors," *Journal of Turbomachinery*, Vol. 117, No. 1, 1995, pp. 62–80. doi:10.1115/1.2835644

[9] Nenni, J. P., and Ludwig, G. R., "A Theory to Predict the Inception of Rotating Stall in Axial Flow Compressors," *7th AIAA Fluid and Plasma Dynamics Conference*, AIAA Paper 1974-528, June 1974.

[10] Sears, W. R., "Rotating Stall in Axial Compressors," *Journal of Applied Mathematics and Physics*, Vol. 6, No. 6, 1955, pp. 429–455. doi:10.1007/BF01600530

[11] Takata, H., and Nagashima, T., "Rotating Stall in Three-Dimensional Blade Rows Subjected to Spanwise Shear Flow," *Proceedings of the 7th International Symposium on Air Breathing Engines*, ISABE Paper 1985-7008, 1985.

[12] Gordon, K., "Three-Dimensional Rotating Stall Inception and Effects of Rotating Tip Clearance Asymmetry in Axial Compressors," Ph.D. Dissertation, Dept. of Aeronautics and Astronautics, Massachusetts Inst. of Technology, Cambridge, MA, 1998.

[13] Sun, X., "On the Relation Between the Inception of Rotating Stall and Casing Treatment," *32th AIAA/ASME/SAE/ASEE Joint Propulsion Conference*, AIAA Paper 1996-2579, July 1996.

[14] Sun, X., Sun, D., and Yu, W., "A Model to Predict Stall Inception of Transonic Axial Flow Fan/Compressors," *Chinese Journal of Aeronautics*, Vol. 24, No. 6, 2011, pp. 687–700. doi:10.1016/S1000-9361(11)60081-2

[15] He, L., "Computational Study of Rotating-Stall Inception in Axial Compressors," *Journal of Propulsion and Power*, Vol. 13, No. 1, 1997, pp. 31–38. doi:10.2514/2.5147

[16] Escuret, J. F., and Garnier, V., "Numerical Simulations of Surge and Rotating Stall in Multi-Stage Axial Flow Compressors," *30th AIAA/ASME/SAE/ASEE Joint Propulsion Conference*, AIAA Paper 1994-3202, June 1994.

[17] Longley, J. P., "Calculating the Flow Field Behaviour of High-Speed Multi-Stage Compressors," *ASME 42nd International Gas Turbine and Aeroengine Congress*, American Society of Mechanical Engineers Paper 97-GT-468, New York, 1997.

[18] Chima, R. V., "A Three-Dimensional Unsteady CFD Model of Compressor Stability," NASA TM-214117, 2006.

[19] Hoying, D. A., Tan, C. S., Huu, D. V., and Greitzer, E. M., "Role of Blade Passage Flow Structures in Axial Compressor Rotating Stall Inception," *Journal of Turbomachinery*, Vol. 121, No. 4, 1999, pp. 735–742. doi:10.1115/1.2836727

[20] Gong, Y., Tan, C. S., Gordon, K. A., and Greitzer, E. M., "A Computational Model for Short-Wavelength Stall Inception and Development in Multi-Stage Compressors," *Journal of Turbomachinery*, Vol. 121, No. 4, 1999, pp. 726–734. doi:10.1115/1.2836726

[21] Gourdain, N., Burguburu, S., Leboeuf, F., and Miton, H., "Numerical Simulation of Rotating Stall in a Subsonic Compressor," *40th AIAA/ASME/SAE/ASEE Joint Propulsion Conference*, AIAA Paper 2004-3929, July 2004.

[22] Jacobs, E. N., and Sherman, A., "Airfoil Section Characteristics as Affected by Variations of the Reynolds Number," NACA TR-586, 1937.

[23] Abbott, I. H., and von Doenhoff, A. E., *Theory of Wing Sections*, 2nd ed., Dover, New York, 1959, pp. 124–185.

[24] Rusak, Z., "Subsonic Flow Around the Leading Edge of a Thin Aerofoil with a Parabolic Nose," *European Journal of Applied Mathematics*, Vol. 5, No. 3, 1994, pp. 283–311. doi:10.1017/S0956792500001479

[25] Rusak, Z., and Morris, W. J., "Stall Onset on Airfoils at Moderately High Reynolds Number Flows," *Journal of Fluids Engineering*, Vol. 133, No. 11, 2011, p. 111104. doi:10.1115/1.4005101

[26] Peskin, C. S., "Flow Patterns Around Heart Valves: A Numerical Method," *Journal of Computational Physics*, Vol. 10, No. 2, 1972, pp. 252–271. doi:10.1016/0021-9991(72)90065-4

[27] Goldstein, D., Handler, R., and Sirovich, L., "Modeling a No-Slip Flow Boundary with an External Force Field," *AIAA Journal*, Vol. 105, No. 2, 1993, pp. 354–366. doi:10.1006/jcph.1993.1081

[28] Cumpsty, N. A., *Compressor Aerodynamics*, 5th ed., Krieger, Malabar, FL, 2004, p. 95.

[29] Wu, C.-H., "A General Theory of Three-Dimensional Flow in Subsonic and Supersonic Turbomachines of Axial-, Radial-, and Mixed-Flow Types," NACA TN-2604, 1952.

[30] Adamczyk, J. J., "Model Equation for Simulating Flows in Multistage Turbomachinery," NASA TM-86869, 1984.

[31] Leboeuf, F., and Trebinjac, I., "Methodology and Results of Analysis for Unsteady Flows in Transonic Turbine and Compressor Stages," *33rd AIAA Fluid Dynamics Conference and Exhibit*, AIAA Paper 2003-3733, June 2003.

[32] Sturmayr, A., and Hirsch, C., "Throughflow Model for Design and Analysis Integrated in a Three-Dimensional Navier–Stokes Solver," *Proceedings of the Institution of Mechanical Engineers, Part A: Journal of Power and Energy*, Vol. 213, No. 4, 1999, pp. 263–273. doi:10.1243/0957650991537608

[33] Xu, L., "Assessing Viscous Body Forces for Unsteady Calculations," *Journal of Turbomachinery*, Vol. 125, No. 3, 2003, pp. 425–432. doi:10.1115/1.1574823

[34] Don, W. S., and Solomonoff, A., "Accuracy and Speed in Computing the Chebyshev Collocation Derivative," NASA CR-4411, 1991.

[35] Rusak, Z., "Transonic Flow Around the Leading Edge of a Thin Airfoil with a Parabolic Nose," *Journal of Fluid Mechanics*, Vol. 248, No. 1, 1993, pp. 1–26. doi:10.1017/S0022112093000667

[36] Namba, M., "Three-Dimensional Flow," AGARD, Rept. AG-298, 1987.

[37] Malik, M. R., "Finite-Difference Solution of the Compressible Stability Eigenvalue Problem," NASA CR-3584, 1982.

[38] Brazier-Smith, P. R., and Scott, J. F., "On the Determination of the Dispersion Equations by Use of Winding Number Integrals," *Journal of Sound and Vibration*, Vol. 145, No. 3, 1991, pp. 503–510. doi:10.1016/0022-460X(91)90119-5

[39] Ivansson, S., Karasalo, I., and Kwok, C. K., "Computation of Modal Numbers Using an Adaptive Winding-Number Integral Method with Error Control," *Journal of Sound and Vibration*, Vol. 161, No. 3, 1993, pp. 173–180. doi:10.1016/0022-460X(93)90410-D

[40] Woodley, B. M., and Peake, N., "Resonant Acoustic Frequencies of a Tandem Cascade. Part 1: Zero Relative Motion," *Journal of Fluid Mechanics*, Vol. 393, No. 1, 1999, pp. 215–240. doi:10.1017/S0022112099005601

[41] Cooper, A. J., Parry, A. B., and Peake, N., "Acoustic Resonance in Aeroengine Intake Ducts," *Journal of Turbomachinery*, Vol. 126, No. 3, 2004, pp. 432–441. doi:10.1115/1.1776586

[42] Press, W. H., Teukolsky, S. A., Vetterling, W. T., Vetterling, W. T., and Flannery, B. P., *Numerical Recipes in Fortran 77: the Art of Scientific Computing*, 5th ed., Cambridge Univ. Press, Cambridge, England, U.K., 2001, Chap. 2.

[43] Nie, C., Xu, G., Cheng, X., and Chen, J., "Micro Air Injection and Its Unsteady Response in a Low-Speed Axial Compressor," *Journal of Turbomachinery*, Vol. 124, No. 4, 2002, pp. 572–579. doi:10.1115/1.1508383

[44] Tong, Z., "The Interactive Unsteady Mechanism Between Tip Leakage Vortex, Stall Inception and Micro Tip Injection in Low-Speed Axial Compressor," Ph.D. Dissertation, Univ. of the Chinese Academy of Sciences, Beijing, 2006.

[45] Stenning, A. H., "Rotating Stall and Surge," *Journal of Fluids Engineering*, Vol. 102, No. 1, 1980, pp. 14–20. doi:10.1115/1.3240618

[46] Moore, R. D., and Reid, L., "Performance of Single-Stage Axial-Flow Transonic Compressor with Rotor and Stator Aspect Ratio of 1.19 and 1.26, Respectively, and with Design Pressure Ratio of 2.05," NASA TP-1659, 1980.

[47] Suder, K. L., "Blockage Development in a Transonic, Axial Compressor Rotor," NASA TM-113115, 1997.

[48] Hoying, D. A., Greitzer, E. M., and Tan, C. S., "Evaluation of Compressor Stall Modeling Assumptions Utilizing Numerical Solutions of Rotating Stall," *33rd AIAA/ASME/SAE/ASEE Joint Propulsion Conference and Exhibit*, AIAA Paper 1997-2771, 1997.

[49] Haynes, J. M., "Active Control of Rotating Stall in a Three Stage Axial Compressor," Gas Turbine Lab., Massachusetts Inst. of Technology, Rept. 218, Cambridge, MA, 1993.

Z. Rusak
Associate Editor